IIETA International Information and Engineering Technology Association
Advancing the World of Information and Engineering

Journal Européen des Systèmes Automatisés
Vol. 59, No. 5, May, 2026, pp. 1235-1245
Journal homepage: http://iieta.org/journals/jesa

Comparative Evaluation of Control Strategies for A Filterless Three-level Grid-Connected Photovoltaic Inverter

Amina Benabda*, Amina Azizi, Amira Lakhdara, Abderrezak Khelfi

Department of Electrical Engineering, Badji Mokhtar-Annaba University, Annaba 23000, Algeria

Corresponding Author Email: amina.benabda@univ-annaba.dz

https://doi.org/10.18280/jesa.590505

Received: 11 March 2026
Revised: 2 May 2026
Accepted: 19 May 2026
Available online: 31 May 2026

Keywords:
photovoltaic system, three-level inverter, filterless grid-connected inverter, Hysteresis Current Control, Pulse Width Modulation Control, Model Predictive Control, hybrid Backstepping-Model Predictive Control, power quality

ABSTRACT

The main objective of this paper is to conduct a comprehensive comparative analysis of several control strategies applied to a three-level grid-connected photovoltaic (PV) inverter operating without a dedicated output filter under variable irradiance conditions. The elimination of the output filter aims to reduce system cost, size, and power losses, while the use of a multilevel inverter structure compensates for the absence of passive filtering by improving the quality of the injected grid current. The investigated control strategies include Hysteresis Current Control (HCC), conventional Pulse Width Modulation (PWM)-based control, Model Predictive Control (MPC), and a hybrid Backstepping-MPC strategy. In this study, the PV source, Direct Current/Direct Current (DC/DC) boost converter, Maximum Power Point Tracking (MPPT) algorithm, and grid synchronization system are considered as a fixed framework, ensuring a fair comparison focused on the inverter current control stage. The performance of each control technique is evaluated in terms of dynamic response and power quality under irradiance fluctuations, based on key performance indicators such as PV power extraction, grid-injected power, current waveform quality, and total harmonic distortion (THD). Simulation results demonstrate that, although PWM and MPC improve system robustness under varying irradiance, the proposed hybrid Backstepping-MPC strategy provides superior overall performance, achieving a current THD of 3.57% and ensuring enhanced dynamic response and strong robustness under irradiance variations.

1. INTRODUCTION

The rapid expansion of photovoltaic (PV) energy conversion systems has intensified research into high-efficiency and high-power-quality grid-connected converters. As the penetration of PV systems continues to increase, ensuring efficient and low-distortion power injection into the utility grid becomes a critical challenge [1]. Among the various power converter topologies, multilevel inverters, particularly three-level Neutral Point Clamped (NPC) structures, offer significant advantages over conventional two-level inverters by reducing voltage stress on semiconductor devices and improving output waveform quality with lower total harmonic distortion (THD) [2, 3].

Traditionally, grid-connected inverters rely on output filters such as Inductor (L), Inductor-Capacitor (LC) and Inductor-Capacitor-Inductor (LCL) filters, to attenuate switching harmonics and meet grid interconnection standards. However, these filters increase system complexity, cost, and losses, and may introduce resonance issues, especially under weak grid conditions. As a result, filterless grid-connected inverter configurations have recently attracted growing attention. In such systems, the control strategy plays a crucial role, as it must compensate for the absence of passive filtering while ensuring high current quality and stable operation under dynamic conditions such as irradiance variations. In this work, the term "filterless" refers to the absence of dedicated LC or LCL output filters, while only the inherent grid inductance, including the line inductance, is considered, without adding any external filtering components.

Several control strategies have been investigated to address these challenges. Classical methods such as Hysteresis Current Control (HCC) are widely used due to their simplicity and fast dynamic response. However, they typically suffer from variable switching frequency and degraded performance under rapid irradiance changes, leading to increased current distortion [4]. Pulse Width Modulation (PWM)-based control strategies offer fixed switching frequency and improved harmonic distortion, but their performance strongly depends on controller tuning and may be limited under highly dynamic conditions.

In contrast, Model Predictive Control (MPC) has emerged as a powerful alternative in power electronics applications. MPC predicts the future behavior of the system and selects the optimal switching state by minimizing a cost function, enabling improved current tracking and reduced THD. Several studies have demonstrated the effectiveness of Finite Control Set Model Predictive Control (FCS-MPC) for grid-connected inverters, including approaches aimed at reducing common-mode voltage and enhancing power quality [5, 6]. Moreover, recent reviews highlight ongoing improvements in MPC design to reduce computational burden and enhance robustness [7].

In addition to linear and predictive approaches, nonlinear control techniques such as backstepping control have shown

strong potential for handling system nonlinearities and ensuring closed-loop stability. Backstepping-based controllers have been successfully applied to grid-connected PV systems, demonstrating robust performance in power regulation and grid synchronization [8].

However, despite the extensive research in this field, several limitations remain. Most existing studies focus on a single control strategy or consider inverter configurations equipped with output filters. The performance of different control techniques under filterless conditions, particularly in the presence of rapid irradiance variations, has not been sufficiently investigated. Furthermore, a fair and systematic comparison between classical, predictive, and hybrid control strategies under identical operating conditions is still lacking. In addition, the potential benefits of combining nonlinear control techniques such as backstepping with MPC have not been fully explored for filterless grid-connected multilevel inverters.

The main novelty of this work lies in the proposed hybrid Backstepping-MPC strategy. Unlike conventional hybrid approaches where controllers were simply combined, the proposed method adopts a hierarchical structure. The backstepping controller first generates a stabilizing reference voltage based on Lyapunov stability theory, ensuring improved dynamic stability. This reference is then tracked by a FCS-MPC, which optimally selects the inverter switching states. This structure allows the simultaneous exploitation of stability guarantees and predictive optimization, resulting in improved robustness, faster transient response, and reduced current distortion under variable irradiance conditions.

In this context, this paper presents a comprehensive comparative study of several control strategies, namely HCC, PWM-based control, MPC, and hybrid Backstepping-MPC approach, applied to a filterless three-level grid-connected PV inverter operating under variable irradiance conditions. In this study, the PV source, DC/DC boost converter, Maximum Power Point Tracking (MPPT) algorithm, Phase-Locked Loop (PLL) synchronization, and load model are considered as a fixed framework. The comparison is strictly focused on the inverter current control strategies to ensure a fair and consistent evaluation.

The performance of each control technique is assessed based on key performance indicators, including PV power extraction, current tracking accuracy, grid-injected power quality, dynamic response under irradiance variations, and THD of both current and voltage.

2. DESCRIPTION AND MODELLING OF THE STUDIED CONFIGURATION

The studied system, shown in Figure 1, is a grid-connected PV conversion system supplying a nonlinear load (PD3). This load is intentionally introduced to generate harmonic distortion and evaluate the robustness of the control strategies under non-ideal operating conditions [9]. The PV array is controlled using the Perturb and Observe (P&O) MPPT algorithm to ensure optimal power extraction under varying irradiance conditions.

The inverter is interfaced with the utility grid through an inductive coupling and operates without a dedicated output filter. Grid synchronization is achieved using a PLL, which provides the grid voltage phase angle required for reference frame transformations and control implementation [10].

A vector-based control framework is adopted for all investigated strategies. The reference currents are generated in the synchronous *dq* reference frame, where the q-axis current reference is set to zero ($i_q = 0$) to guarantee unity power factor operation. These reference currents are then transformed back into the three-phase stationary frame using the inverse Park transformation, yielding the three-phase current references applied to the inverter current controller.

To ensure a fair and consistent comparison, the same system configuration, MPPT algorithm, PLL, current reference generation scheme, and operating conditions are maintained for all cases. Only the inverter current control strategy is varied, including:

- HCC
- Conventional PWM-based control
- MPC
- Hybrid Backstepping-MPC control

All controllers are tuned to ensure stable and comparable performance under identical conditions.

This approach enables a direct and objective evaluation of the impact of each control strategy on PV power extraction, grid-injected power, current waveform quality, and THD under variable irradiance conditions.

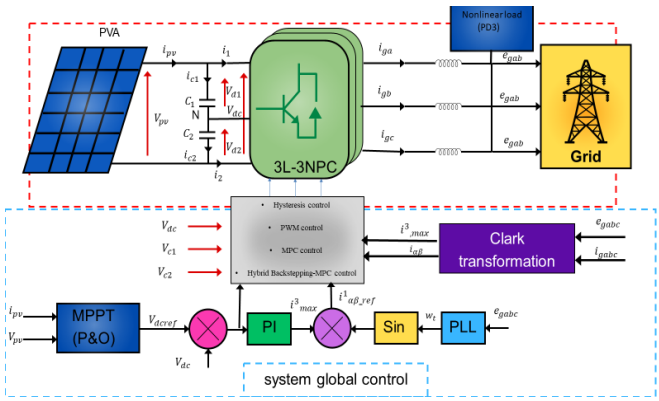

Figure 1. Block diagram of the complete photovoltaic (PV) system and the control strategy

2.1 Modelling a photovoltaic panel

A PV field based on PV panels is considered and simulated by modelling the elementary cell with a single diode, as shown in Figure 2. The PV cell is presented as an electric current generator whose behaviour is equivalent to a shunt current source with a diode. The main equation of the cell is given by [11]:

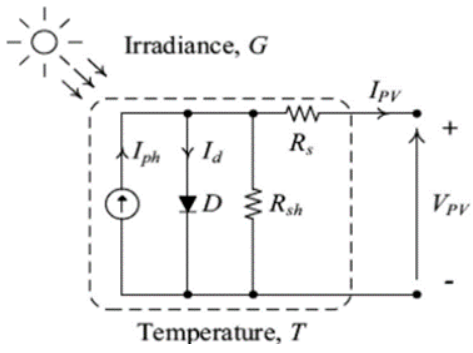

Figure 2. Model of a photovoltaic (PV) solar panel

$$I_{pv} = I_{ph} - I_{sat}\left[exp\left(\frac{(V_{pv} + (I_{pv}R_{Ser}))}{nKT}\right) - 1\right] - \frac{V_{pv} + (I_{pv}R_{Ser})}{R_{shu}} \quad (1)$$

I_{pv}: PV output current (A)
I_{ph}: Photogenerated current (A)
I_{sat}: Diode reverse saturation current (A)
V_{pv}: PV output voltage (V)
R_{ser}: Series resistance (Ω)
R_{shu}: Shunt resistance (Ω)
n: Diode ideality factor (dimensionless, typically 1-2)
K: Boltzmann constant (1.38×10^{-23} J/k)
T: Cell temperature (k)
The main PV parameters are given in Table 1.

Table 1. Photovoltaic (PV) parameters

Parameter	Symbol	Value
Number of series modules	Ns	16
Number of parallel strings	Np	9
Open circuit voltage	Voc	36.6 V
Short-circuit current	Isc	7.97 A
Voltage at Maximum Power Point (MPP)	Vmp	29.3 V
Current at MPP	Imp	7.47 A

2.2 Converter

To obtain the best return on the electrical energy produced/solar energy received by a PV installation, a DC/DC converter must be used to ensure that the PV module is always operating at its optimum power. To do this, we use a specific converter with MPPT control, enabling the module to operate at optimum voltage and optimum current, and therefore at optimum power [12].

The relation between input and output voltages of the boost converter is given as:

$$V_{out} = \frac{1}{1-D}V_{in} \quad (2)$$

With D is the duty cycle, which is given as:

$$D = \frac{T_{on}}{T_s} \quad (3)$$

The parameters of the boost DC–DC converter used in this study are summarized in Table 2.

Table 2. Boost converter parameters

Parameter	Symbol	Value
Inductance	L_b	4.5 mH
Capacitance	C_b	5000 µF
Sampling time	T_s	10 µs

2.3 Maximum Power Point Tracking command (P&O algorithm)

The P&O is a well-known MPPT technique favored for its simplicity. It operates by continuously perturbing the operating voltage and observing the impact on output power. Based on the signs of the change in power (ΔP) and the change in voltage (ΔV), calculated from the voltage (V) and current (I) inputs, the algorithm decides how to adjust the duty cycle (D) to reach the Maximum Power Point (MPP). The flowchart in this method is shown in Figure 3 [13, 14]:

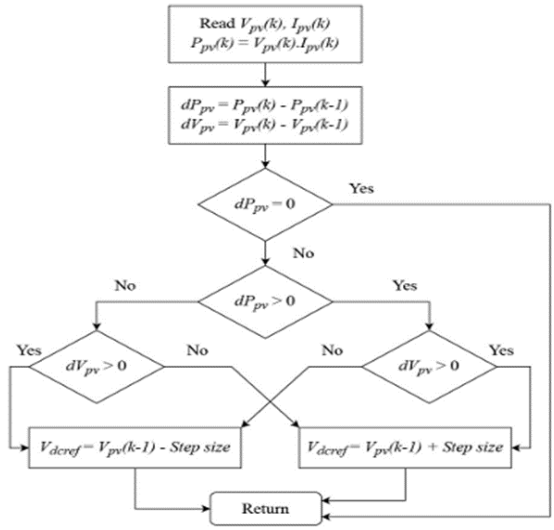

Figure 3. Perturb and observe (P&O) flowchart

3. DC/AC CONVERTERS FOR PHOTOVOLTAIC SYSTEMS

Multilevel inverters play a key role in energy conversion, particularly for applications requiring high voltage and power. Unlike conventional structures, these inverters generate an output voltage closer to a sine wave, thereby reducing harmonic distortion and improving energy efficiency. Their advanced design offers significant advantages in terms of efficiency, reduced stress on components, and compatibility with modern electrical networks. Thanks to these features, multilevel inverters are widely adopted in various fields such as grid-connected PV systems, high-power industrial drives, electric traction, and smart grids [15-17].

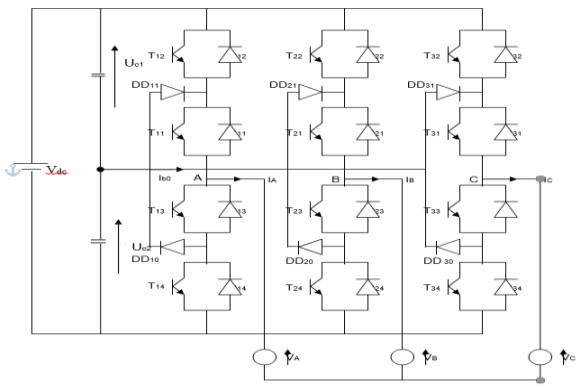

Figure 4. Three-level Neutral Point Clamped (NPC) inverter

Among multilevel inverter topologies, the three-level Neutral Point Clamped (NPC) inverter shown in Figure 4 has gained significant attention due to its balanced compromise between performance, complexity, and reliability. By introducing an additional voltage level through a clamped

neutral point, the NPC inverter is capable of generating three discrete output voltage levels ($+\frac{V_{DC}}{2}, 0, -\frac{V_{DC}}{2}$), which significantly reduces harmonic distortion compared to conventional two-level inverters. Moreover, the three-level NPC structure allows for lower voltage stress across the power switches, making it particularly suitable for grid-connected PV systems operating at medium and high power levels.

3.1 Hysteresis Current Control

In this control strategy, the inverter currents are regulated directly in the three-phase abc reference frame. The reference currents are obtained from the inverse Park transformation applied to the dq-axis current references.

3.1.1 Current error definition

The current tracking errors for each phase are defined as:

$$e_a = i_a^* - i_a \tag{4}$$

$$e_b = i_b^* - i_b \tag{5}$$

$$e_c = i_c^* - i_c \tag{6}$$

where, i_x^* and i_x denote the reference and measured phase currents, respectively, with

$$x \in \{a, b, c\}$$

3.1.2 Hysteresis band

A fixed hysteresis band (h) is imposed on the current errors that:

$$|e_x| \leq h \tag{7}$$

$$x \in \{a, b, c\}$$

The controller aims to maintain the phase currents (i_a, i_b and i_c) within this predefined hysteresis band around their references.

3.1.3 Switching law principle

The switching decisions are made according to the following rule:

- $if\ e_x > h$, the phase voltage is increased to force the current to decrease its error.
- $if\ e_x < -h$, the phase voltage is decreased to force the current to decrease its error.

For a three-level NPC inverter, the available phase voltage levels are given by:

$$v_x \in \left\{+\frac{V_{dc}}{2}, 0, -\frac{V_{dc}}{2}\right\} \tag{8}$$

The appropriate voltage level is selected in real time to ensure fast current tracking and to keep the current within the hysteresis bounds. The hysteresis bandwidth h is selected as a compromise between current ripple and switching frequency.

3.2 Pulse Width Modulation control of the three-level inverter

In the conventional PWM control strategy for the three-level NPC inverter, the reference current is first processed through a proportional-integral (PI) controller to generate the reference voltage [18, 19].

The PI controller is defined as:

$$V_x^{ref} = Kp(i_x^* - i_x) + Ki \int (i_x^* - i_x)dt \tag{9}$$

The reference voltage is then compared with two triangular carrier signals, one for the upper switch (Vc+) and one for the lower switch (Vc-), to generate the switching signals:

$$\begin{aligned} &S_1 = 1, \mathrm{S_2}{=}0, \mathrm{V}_{ref} > Vc + \ (\text{output } \frac{V_{dc}}{2}) \\ &S_1 = 1, \mathrm{S_2}{=}1, \mathrm{Vc}{-}{<}\mathrm{V}_{ref} < Vc + \ (\text{output } 0) \\ &S_3 = 1, \mathrm{S_4}{=}0, \mathrm{V}_{ref} < Vc - \ (\text{output } -\frac{V_{dc}}{2}) \end{aligned} \tag{10}$$

Finally, the phase voltage applied to the load is calculated as:

$$V_{\text{phase}} = \begin{cases} +\frac{V_{dc}}{2}, \mathrm{S_1} = 1 \text{ and } \mathrm{S_2} = 0 \\ 0, (\mathrm{S_1} = 1 \text{ and } \mathrm{S_2} = 1) \text{ or } (\mathrm{S_3} = 1 \text{ and } \mathrm{S_4} = 1) \\ -\frac{V_{dc}}{2}, \mathrm{S_3} = 1 \text{ and } \mathrm{S_4} = 0 \end{cases} \tag{11}$$

This approach ensures a fixed switching frequency and improved harmonic performance compared to hysteresis control.

3.3 Model Predictive Control control strategy

In the proposed MPC-PI control strategy for the three-level NPC inverter, the future grid currents are predicted using a discrete-time model of the inverter:

$$i_x(k+1) = i_x(k) + \frac{T_s}{L_g}(V_x(k) - V_{grid} - R_g i_x(k)) \tag{12}$$

where, $i_x(k)$ is the output current at the sampling instant k, $V_x(k)$ is the inverter output voltage, V_{grid} is the grid voltage, and L_g, R_g are the series inductance and resistance of the grid.

The sampling time T_s is kept identical for all control strategies to ensure a fair comparison.

The control objective is to minimize the tracking error between the predicted grid currents and the three-phase reference currents Iref, generated through the inverse Park transformation, in order to ensure unity power factor:

$$J = \sum_{x=a,b,c} (i_x^* - i_x(k+1))^2 + \lambda \Delta S \tag{13}$$

i_x^*: reference grid current of phase x.

i_x (k+1): predicted grid current of phase x at the next sampling instant.

λ: weighting factor used to penalize switching activity.

ΔS: switching variation term, representing the change in inverter switching states between two consecutive sampling instants.

$$\Delta S = \sum | S(k) - S(k-1) | \tag{14}$$

where,

S(k): inverter switching state at sampling instant k.

S(k-1): inverter switching state at the previous sampling instant.

At each sampling instant, the optimal switching state is selected from the set of all admissible inverter states U by minimizing the cost function:

$$S_{opt}(k) = arg \min_{S(k)\in U} J \tag{15}$$

The cost function is designed to minimize the current tracking error while limiting the switching frequency through the weighting factor λ, ensuring a trade-off between tracking performance and switching losses [20-25].

3.4 Backstepping-MPC control strategy

To further enhance the dynamic performance and robustness of the grid-connected three-level NPC inverter operating without an output filter, a hybrid Backstepping-MPC strategy is adopted. This approach combines the stability guarantees of nonlinear backstepping control with the optimal switching selection capability of MPC [26].

In contrast to conventional MPC approaches, the proposed strategy integrates a backstepping-based reference voltage within the predictive control framework. This intermediate control variable, derived from Lyapunov stability theory, ensures a stable control objective before the optimization stage. As a result, the MPC is used not only for current tracking but also for selecting the optimal switching state that best approximates the stabilizing control action, thereby improving dynamic performance and robustness.

This structure ensures that stability is guaranteed by the backstepping stage, while the MPC optimizes the switching states to accurately track the stabilizing reference.

However, the computational burden remains manageable due to the finite number of switching states in the FCS-MPC framework.

3.4.1 Phase current dynamic model

Considering the coupling inductance L_g and resistance R_g of grid, the dynamic model of each phase current can be expressed as:

$$L_g \frac{di_x}{dt} = v_x - v_{g,x} - R_g i_x \tag{16}$$

where,

- v_x is the inverter output phase voltage
- $v_{g,x}$ is the grid phase voltage
- i_x is the grid current

$$x \in \{a, b, c\}$$

3.4.2 Backstepping control design

The current tracking error for each phase is defined as:

$$e_x = i_x - i_x^* \tag{17}$$

A Lyapunov candidate function is chosen as:

$$V = \frac{1}{2} e_x^2 \tag{18}$$

Taking the derivative of V and substituting the system dynamic yields:

$$\frac{dV}{dt} = e_x\left(\frac{1}{L_g}(v_x - v_{g,x} - R_g i_x) - i_x^*\right) \tag{19}$$

To ensure asymptotic stability $\frac{dv}{dt}$, the virtual control is defined as:

$$v_x^{ref} = v_{g,x} + R_g i_x + L_g i_x^* - k e_x \tag{20}$$

where, k > 0 is a backstepping gain.

This reference voltage guarantees exponential convergence of the current tracking error.

3.4.3 Integration with Model Predictive Control

Since the inverter can only generate a finite number of voltage levels, the continuous reference voltage V_x^{ref} cannot be applied directly. Therefore, FCS-MPC is used to select the optimal switching state.

The discrete-time prediction model is given by:

$$i_x(k+1) = i_x(k) + \frac{T_s}{L_g}(v_x^{ref}(k) - v_{g,x}(k) - R_g i_x(k)) \tag{21}$$

For each admissible switching state of the three-level NPC inverter, the predicted current is computed and evaluated using the following cost function:

$$J = \sum_{x=a,b,c} (i_x^* - i_x(k+1))^2 + \lambda \Delta S \tag{22}$$

The switching state that minimizes the cost function while producing a voltage vector closest to V_x^{ref} is applied during the next sampling period.

4. SIMULATION RESULTS

The studied system is connected to the utility grid through a three-level Neutral-Point-Clamped (NPC) inverter and supplies a nonlinear load (PD3) to introduce harmonic disturbances. The DC-link voltage is regulated at 800 V to ensure proper inverter operation and stable power transfer. Different control strategies are applied to the same inverter topology in order to evaluate their impact on system performance under variable irradiance conditions. The analysis focuses on key performance indicators, including THD of voltage and current, grid-injected power, PV power, load power, as well as grid voltage and current waveforms.

PV power extraction is ensured using the P&O MPPT algorithm, while grid synchronization is achieved using a PLL. The PLL parameters are set to Kp = 120 and Ki = 2000, with a sampling time Ts = 1×10^{-5} s. The switching frequency is fixed and derived from the sampling time (Fs = 1/Ts = 100 kHz). The system is connected to a utility grid modeled with a nominal RMS line-to-line voltage of 415 V and a frequency of 50 Hz; the grid impedance is represented by an inductance L_g = 3 mH and a resistance R_g = 0.2 Ω, which model the combined effects of the line and the grid, and do not correspond to a dedicated output filter. All simulations are carried out in

MATLAB/Simulink.

To assess the performance and robustness of the considered control strategies, the system is evaluated under dynamic operating conditions characterized by rapid irradiance variations. The known performance limitations of HCC under such transient conditions justify the need for a comparative investigation of alternative approaches, including PWM-based control, MPC, and a hybrid Backstepping-MPC strategy.

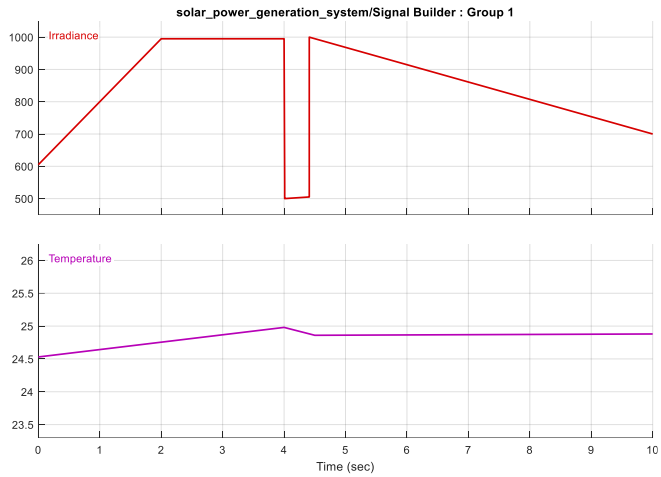

Figure 5. Irradiance and temperature profiles

Figure 5 illustrates the irradiance and temperature profiles applied to the PV system. The irradiance starts at 600 W/m^2, increases progressively to 1000 W/m^2 at 2 s, and remains constant until 4 s. A sudden decrease to 500 W/m^2 occurs between 4 s and 4.5 s, followed by a rapid recovery back to 1000 W/m^2 at 4.5 s. Afterwards, the irradiance gradually decreases to approximately 700 W/m^2 at 10 s. The temperature varies slightly between 24.5 °C and 25 °C, reaching its maximum around 4 s, indicating a negligible impact compared to irradiance variations.

The PV power response under variable irradiance is shown in Figure 6. The PV power reaches approximately 31 kW under maximum irradiance conditions. When HCC is applied, the PV power is significantly perturbed during irradiance transitions, exhibiting strong oscillations and slow recovery. This behavior reflects the limited ability of a hysteresis control to ensure stable power extraction under rapidly changing environmental conditions. Starting from PWM-based control, a clear improvement is observed: the PV power becomes more stable, with reduced oscillations and improved tracking of the MPP. This performance is further enhanced with MPC and reaches its best level with the hybrid Backstepping-MPC strategy, which ensures smooth and fast PV power stabilization under irradiance variations.

A clear power dip is observed between 4 s and 4.5 s, corresponding to the sudden drop in irradiance. This dip reflects the transient mismatch between the PV array operating point and the MPP under rapidly changing environmental conditions.

Figure 7 presents the grid-injected power for the different control strategies. Under hysteresis control, the grid power is strongly disturbed during periods of PV power instability. During these intervals, the grid temporarily supplies power to the load, which explains the observed reversal of power flow: the grid behaves as a power source instead of a power sink. This phenomenon highlights the poor coordination between PV generation and grid power injection under hysteresis control.

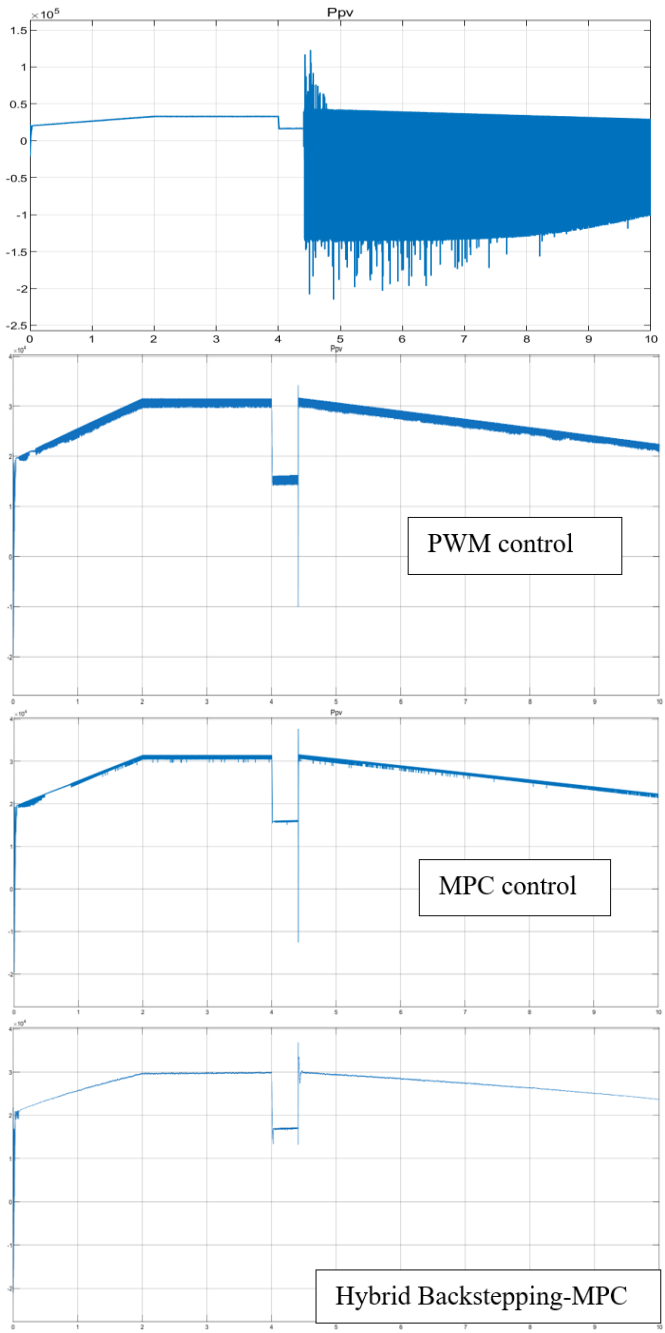

Figure 6. Photovoltaic (PV) power

The grid-injected power reaches approximately 22 kW; from PWM-based control onward, the grid power becomes significantly more stable. The grid consistently absorbs the power delivered by the PV system, with reduced oscillations. The MPC and hybrid Backstepping-MPC strategies further improve power smoothness, ensuring reliable and continuous power transfer to the grid.

The proposed method exhibits faster transient response and reduced power oscillations compared to other strategies. The corresponding grid current waveforms are depicted in Figure 8. Under hysteresis control, the grid current exhibits noticeable distortion and increased ripple especially during irradiance transitions. With the application of PWM-based control, the current waveform becomes more regular and closer to a sinusoidal shape. This improvement is reinforced by MPC and

is most pronounced with the hybrid Backstepping-MPC strategy, which provides quasi-sinusoidal grid currents with accurate reference tracking, even under rapid irradiance changes.

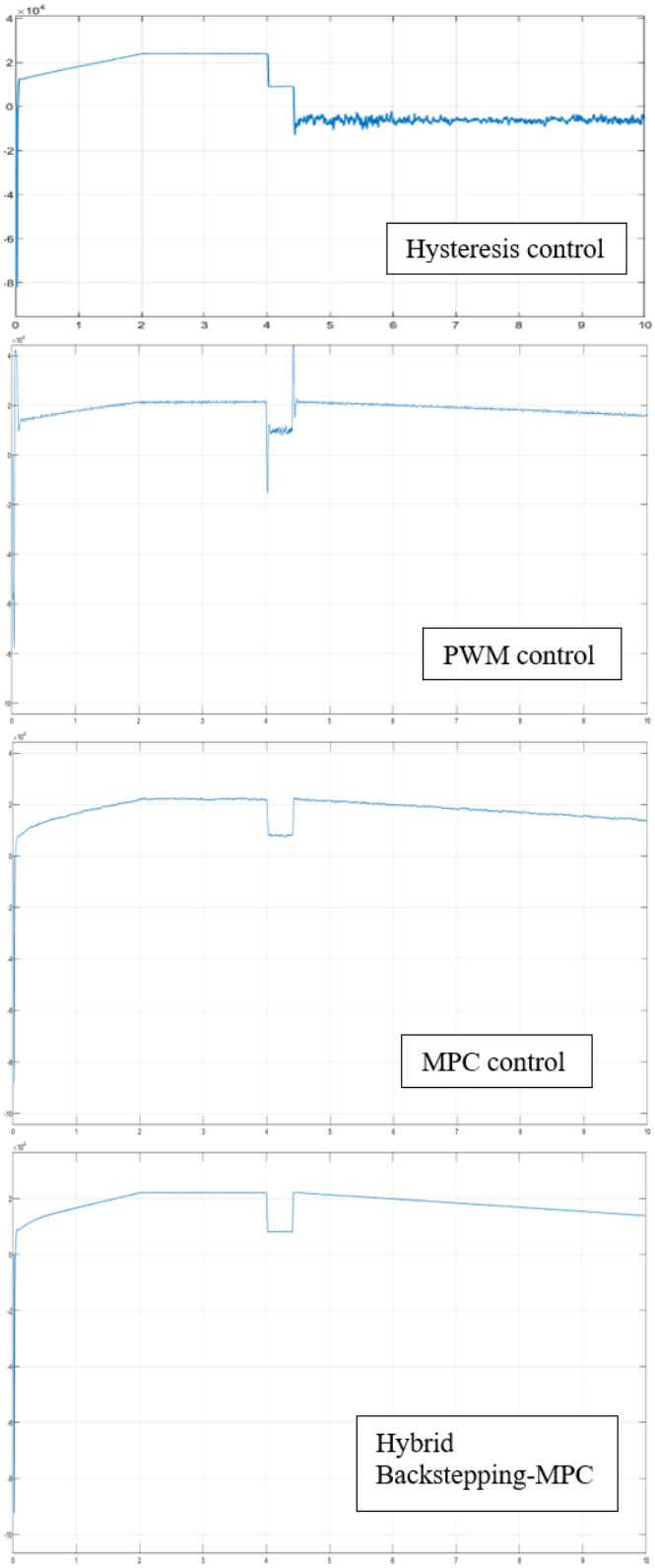

Figure 7. Grid-injected power

Figure 9 presents the load power profiles under the investigated control strategies. The nonlinear load contributes to harmonic distortion, making the evaluation of current quality more representative of practical operating conditions.

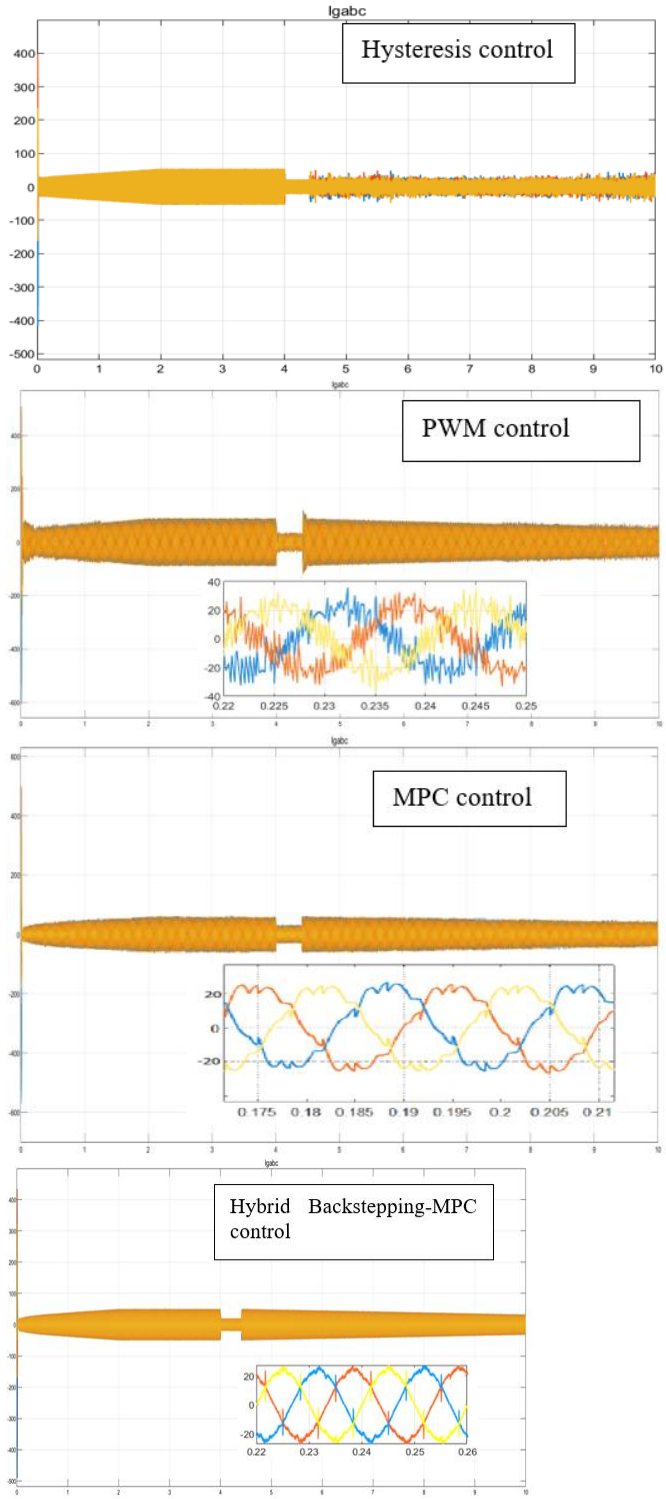

Figure 8. Grid current waveform

The load power remains essentially constant at approximately 5.8 kW for all cases, indicating that the load demand is continuously satisfied regardless of the applied control strategy. This observation confirms that the comparative analysis primarily reflects differences in power quality, power flow dynamics, and current regulation, rather than variations in load supply. Figure 10 shows the grid voltage waveforms for the different control strategies. It can be observed that the grid voltage remains practically identical for all control methods. This result confirms that the utility grid voltage is imposed by the grid itself and is not significantly affected by the inverter control strategy, despite the absence of an output filter.

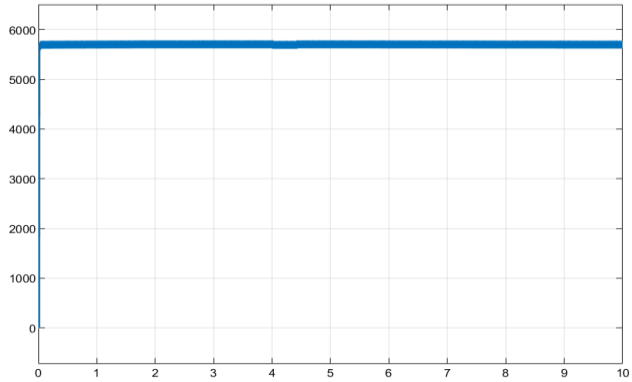

Figure 9. Load power profiles under different control strategies

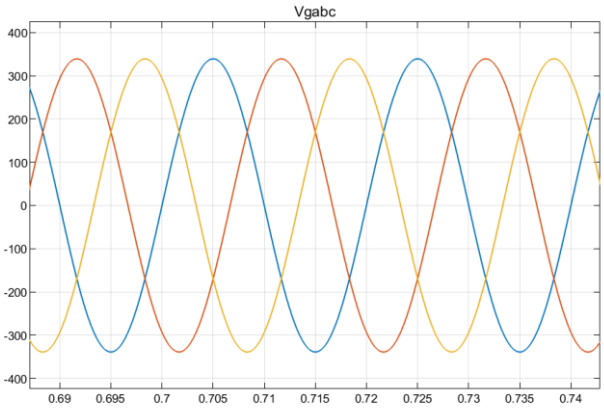

Figure 10. Grid voltage waveform under different control strategies

Figure 11 illustrates the THD of the grid current obtained using Fast Fourier Transform (FFT) analysis. The results show a clear reduction in THD when moving from hysteresis control to more advanced control strategies:

- Hysteresis control: highest distortion level (30.81%)
- PWM-based control: reduced THD (8.36%)
- MPC: further improvement (5.09%)
- Backstepping-MPC: lowest THD (3.57%)

Compared to MPC, the proposed method reduces the current THD by approximately 30%, highlighting its superior performance.

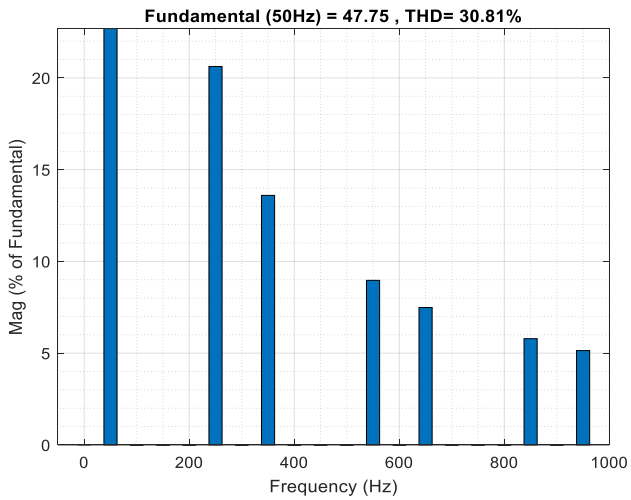

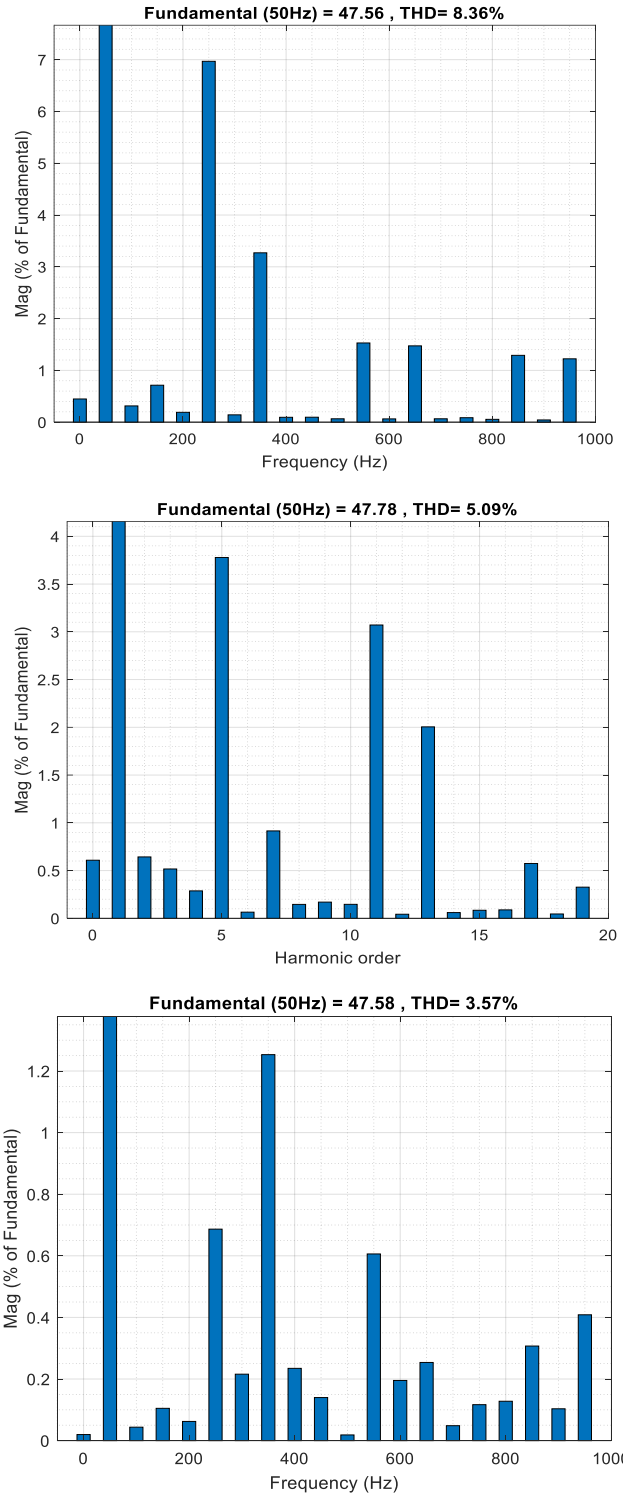

Figure 11. Total harmonic distortion (THD) of the grid current under hysteresis control

Figure 12 shows the THD of the grid voltage for the different control strategies. Under HCC, the voltage THD reaches 0.13%, which reflects the impact of distorted grid currents on the voltage quality at the point of common coupling. When PWM-based and MPC strategies are applied, the voltage THD is significantly reduced to 0.04% and 0.03%, respectively, indicating improved current regulation and reduced harmonic injection. The hybrid Backstepping-MPC strategy achieves the lowest voltage THD, on the order of 0.04×10^{-3}, demonstrating its excellent capability to preserve grid voltage quality, even in a filterless inverter configuration.

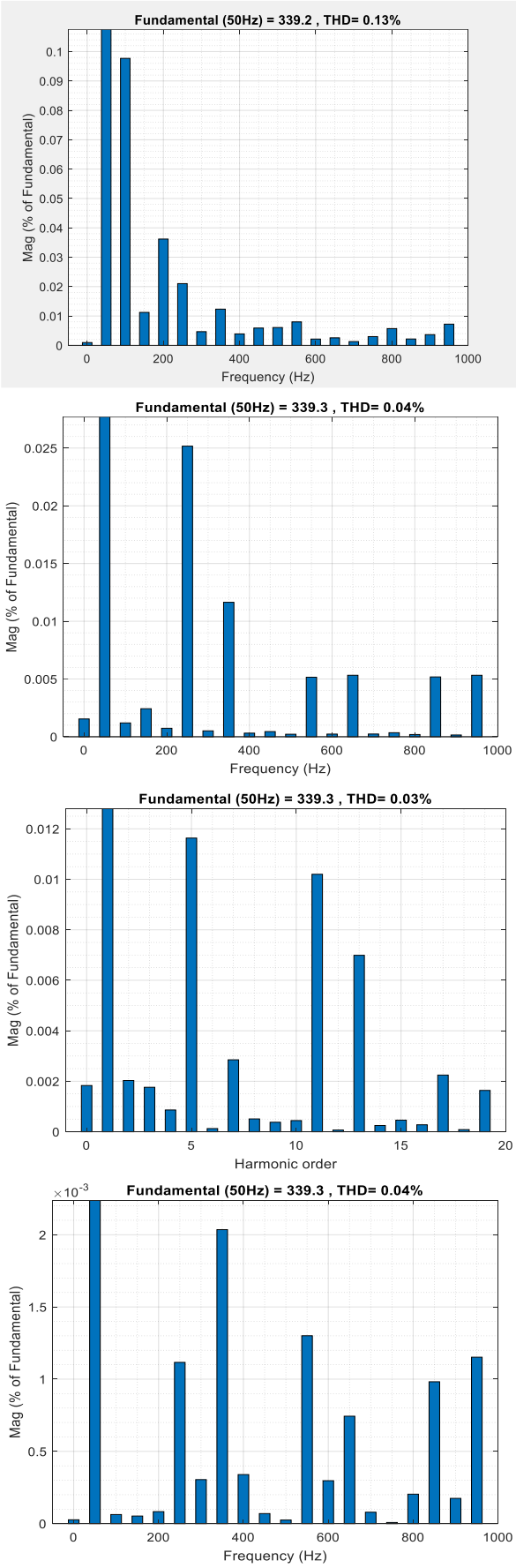

Figure 12. Total harmonic distortion (THD) of the grid voltage

The THD values corresponding to the different control strategies are reported in Table 3. All values are obtained using FFT analysis.

Table 3. Voltage and current total harmonic distortion (THD) under variable irradiance conditions

Control Strategy	Current THD (%)	Voltage THD (%)
Hysteresis Current Control (HCC)	30.81	0.13
PWM-based control	8.36	0.04
Model Predictive Control (MPC)	5.09	0.03
Hybrid Backstepping-MPC control	3.57	0.04×10^{-3}

5. CONCLUSION

The present study provides a comprehensive comparative analysis of four current control strategies applied to a filterless three-level grid-connected PV inverter operating under variable irradiance conditions. The investigated controllers include HCC, PWM-based control, MPC, and a hybrid Backstepping-MPC strategy. The analysis was carried out under identical system conditions, where the PV source, DC-DC boost converter, MPPT algorithm, and grid synchronization system were kept unchanged, ensuring a fair evaluation focused exclusively on the inverter current control stage.

The results show that HCC offers fast dynamic response but suffers from variable switching frequency and increased current ripple under rapid irradiance variations. PWM control improves switching behavior and reduces harmonic distortion; however, its performance remains sensitive to controller tuning and operating conditions. MPC demonstrates improved current tracking and reduced THD due to its optimization-based decision mechanism, although its performance may still be limited under strong nonlinearities and fast transient variations.

The proposed hybrid Backstepping-MPC strategy overcomes these limitations by combining the advantages of nonlinear stabilization and predictive optimization. The backstepping controller ensures system stability and provides a stabilizing reference based on Lyapunov theory, while the MPC ensures optimal switching state selection to accurately track this reference. This hierarchical structure significantly improves dynamic response, enhances robustness against irradiance fluctuations and achieves superior current quality with reduced THD below the IEEE limit of 5%, despite the absence of an output filter.

Future work will focus on extending the study to more complex grid conditions and improving control performance under nonlinear loads.

REFERENCES

[1] Ponnambalam, S., Ilampoornan, M.K. (2025). Effects, challenges, and issues for integration of solar PV systems to the grid. In Explainable Artificial Intelligence and Solar Energy Integration, pp. 87-114.

[2] Gada, S., Fekik, A., Mahdal, M., Vaidyanathan, S., Maidi, A., Bouhedda, A. (2023). Improving power quality in grid-connected photovoltaic systems: A comparative analysis of model predictive control in three-level and two-level inverters. Sensors, 23(18): 7901. https://doi.org/10.3390/s23187901

[3] Abdelhak, L., Anas, B., Jamal, B., Kamal, H., Mostafa, E.O. (2025). A multilevel PV inverter control with minimal total harmonic distortion (THD). In Pioneering Sustainable Innovations in Renewable Energy Technologies, pp. 1-18. https://doi.org/10.4018/979-8-3693-9924-8.ch001

[4] Cai, S.L., Li, D.X., Shao, S.Y., Yang, X.Y., Zhang, Q., Cheng, P.Y. (2024). A digital hysteresis control method for three-level grid-tie inverter based on online prediction of sampling time without inductance. Frontiers in Energy Research, 12: 1403346. https://doi.org/10.3389/fenrg.2024.1403346

[5] Bebboukha, A., Meneceur, R., Chouaib, L., Anees, M.A., et al. (2024). Finite control set model predictive current control for three-phase grid connected inverter with common mode voltage suppression. Scientific Reports, 14: 19832. https://doi.org/10.1038/s41598-024-71051-9

[6] Bebboukha, A., Chouaib, L., Meneceur, R., Elsanabary A., Anees, M.A., Mekhilef, S., Zaitsev, I., Bajaj, M., Bereznychenko, V. (2024). A reduced vector model predictive controller for a three-level neutral point clamped inverter with common-mode voltage suppression. Scientific Reports, 14: 15180. https://doi.org/10.1038/s41598-024-66013-0

[7] Mirza, S., Hussain, A. (2024). New approaches in finite control set model predictive control for grid-connected photovoltaic inverters: State of the art. Solar, 4(3): 491-508. https://doi.org/10.3390/solar4030023

[8] El Madani, Z., Yahya, A., El Malki, Z. (2024). Nonlinear backstepping control for three-phase single-stage grid-tied photovoltaic systems via an LCL-filter. Engineering, Technology & Applied Science Research, 14(6): 17950-17957. https://doi.org/10.48084/etasr.8722

[9] Tweve, E., Kichonge, B., Kivevele, T. (2025). Impacts of nonlinear loads on the power quality of solar microgrids and proposed mitigation strategies. Energy Science & Engineering, 13(4): 1960-1982. https://doi.org/10.1002/ese3.70019

[10] Guerrero-Rodríguez, N.F., Ramírez-Rivera, F.A., Batista-Jorge, R.O., Ferreira, J.A., Mercado-Ravelo, R. (2025). Comparative study of the grid current harmonic attenuation in a photovoltaic generator due to the influence of the synchronization strategy. International Journal of Electrical and Computer Engineering Systems, 16(6): 431-441. https://doi.org/10.32985/ijeces.16.6.1

[11] Benabda, A., Kelaiaia, M.S., Labar, H., Logerais, P.O., Durstanti, J.F. (2017). Boost chopper MPP assessment based on solar irradiance and predictive duty cycle applied to a PV system. International Journal of Hydrogen Energy, 42(30): 19403-19414. https://doi.org/10.1016/j.ijhydene.2017.06.033

[12] Yang, P.C., Peng, Y.G., Xia, Y.H., Wei, W., Yu, M., Feng, Q.F. (2022). A unified bus voltage regulation and MPPT control for multiple PV sources based on modified MPC in the DC microgrid. Frontiers in Energy Research, 10: 1010425. https://doi.org/10.3389/fenrg.2022.1010425

[13] Li, Z.H., Dewantoro, G., Xiao, T.H., Swain, A. (2025). A comparative analysis of fuzzy logic control and model predictive control in photovoltaic maximum power point tracking. Electronics, 14(5): 1009. https://doi.org/10.3390/electronics14051009

[14] Bouksaim, M., Mekhfioui, M., Srifi, M.N. (2025). A comprehensive decade-long review of advanced MPPT algorithms for enhanced photovoltaic efficiency. Solar, 5(3): 44. https://doi.org/10.3390/solar5030044

[15] Vaidya, S., Prasad, K., Kilby, J. (2025). The role of multilevel inverters in mitigating harmonics and improving power quality in renewable-powered smart grids: A comprehensive review. Energies, 18(8): 2065. https://doi.org/10.3390/en18082065

[16] Tkouti, N., Rahoua, N., Mechgoug, R. (2024). Comparative study between three and seven multilevel inverter for grid-connected photovoltaic (PV) system controlled by PI regulator. Studies in Engineering and Exact Sciences, 5(2): e6709.

[17] Benabda, A., Azizi, A. (2025). Comparative study of the different structures of multi-level inverters for the connection of pv systems to the power grid. In 2025 International Conference on Artificial Intelligence, Embedded Systems, and Renewable Energy (AIESRE), Tizi-Ouzou, Algeria, pp. 1-7. https://doi.org/10.1109/AIESRE67541.2025.11470205

[18] Singh, A., Bhandari, S., Kumar, J. (2024). Suppression of harmonics in a novel multilevel inverter using multi-carrier based PWM technique. Journal of Electrical Engineering & Technology, 19: 5027-5043. https://doi.org/10.1007/s42835-024-01907-7

[19] Wang, K., Zheng, Z.D., Xu, L., Li, Y.D. (2021). Neutral-point voltage balancing method for five-level NPC inverters based on carrier-overlapped PWM. IEEE Transactions on Power Electronics, 36(2): 1428-1440.

[20] Choudhury, S., Sahu, J.B., Nayak, B. (2022). Power tracking capability enhancement of a grid-tied partially shaded photovoltaic system through MPC based maximum power point technique. International Journal of Renewable Energy Research, 12(2): 1000-1012.

[21] Zhang, Z., Ma, J., Qiu, L., Liu, X., Rodríguez, J., Fang, Y. (2025). A novel neural network-assisted finite-set subspace predictive control method for 3L-NPC converters. IEEE Transactions on Industrial Electronics, 72(12): 12039-12051. https://doi.org/10.1109/TIE.2025.3574521

[22] Zaid, S.A., Bakeer, A., Albalawi, H., Alatwi, A.M., Abdeldaim, H., Manqarah, B. (2023). Model-free predictive current control of a 3-φ grid-connected neutral-point-clamped transformerless inverter. Energies, 16(7): 3141. https://doi.org/10.3390/en16073141

[23] Lakhdari, A., Benlahbib, B., Abdelkrim, T. (2022). Model predictive control for three-phase three-level NPC inverter based APF interfacing single stage photovoltaic system to the grid. Journal Européen des Systèmes Automatisés, 55(1): 25-34. https://doi.org/10.18280/jesa.550103

[24] Alharbi, Y., Darwish, A., Ma, X.D. (2025). A review of model predictive control for grid-connected PV applications. Electronics, 14(4): 667.

[25] Silveira, K., Grigoletto, F.B., Carnielutti, F., Aly, M., Norambuena, M., Rodriguez, J. (2025). Model predictive control of common ground PV multilevel inverter with sliding mode observer for capacitor voltage estimation. Processes, 13(9): 2961. https://doi.org/10.3390/pr13092961

[26] Aslan, M., Afif, B., Salmi, M., Merabet, B., Berka, M., Masoud, S.A. (2024). Performance enhancement of microgrid systems using backstepping control for grid

side converter and MPPT optimization. Solar Energy and Sustainable Development Journal, 14(1): 19-41. https://doi.org/10.51646/jsesd.v14i1.367

NOMENCLATURE

I_{ph}	Photogenerated current, A
I_{pv}	PV output current, A
I_{sat}	Diode reverse saturation current, A
V_{pv}	PV output voltage, V
D	Duty cycle, dimensionless
V_{dc}	DC-link voltage, V
i_x	Grid current of phase x, A
i_x^*	Reference grid current of phase x, A
i_x(k+1)	Predicted grid current at next sampling instant, A
V_x	Inverter output phase voltage, V
V_x^{*ref}	Reference phase voltage, V
$V_{g,x}$	Grid phase voltage, V
L_g	Grid inductance, H
R_g	Grid resistance, Ω
Kp	Proportional gain, dimensionless
Ki	Integral gain, dimensionless
Ts	Sampling time, s
J	Cost function, dimensionless
Λ	Weighting factor, dimensionless
ΔS	Switching variation, dimensionless
K	Backstepping gain, dimensionless
X	Phase index (a, b, c)
g	Grid
pv	Photovoltaic
ref	Reference value
DC	Direct Current